ELSEVIER

Journal of Magnetism and Magnetic Materials 200 (1999) 392–404

Journal of magnetism and magnetic materials

www.elsevier.com/locate/jmmm

Hard/soft magnetic heterostructures: model exchange-spring magnets

Eric E. Fullerton[a,*], J.S. Jiang[b], S.D. Bader[b]

[a]*IBM Almaden Research Center, 650 Harry Road, San Jose, CA 95120, USA*
[b]*Materials Science Division, Argonne National Laboratory, Argonne, IL 60439, USA*

Received 17 February 1999; received in revised form 2 April 1999

Abstract

An overview is provided of research on exchange-spring coupled magnetic films and multilayers, including fabrication methods, and the characterization and modeling of the magnetization reversal processes. For coupled hard/soft bilayers and multilayers the deposition process provides nanometer-scale control of thicknesses and magnetic anisotropy. Such magnetic heterostructures provide model systems for studying the exchange hardening mechanism. Recent work on epitaxial SmCo/Fe and SmCo/Co bilayers and superlattices that display many of the characteristic features of exchange-spring magnets is highlighted. Comparison of the experimental results with numerical simulations indicates that the exchange-spring behavior can be understood from the intrinsic parameters of the hard and soft layers. The simulations are extended to realistically estimate the ultimate gain in performance that can potentially be realized in permanent magnets based on the exchange-spring principle.

Keywords: Heterostructures; Magnetic films; Magnetic multilayers; Exchange-spring magnets

1. Introduction

The figure of merit for a permanent magnet material is the maximum energy product $(BH)_{max}$ that is twice the maximum magnetostatic energy available from a magnet of optimal shape. The product tends to increase both with increasing coercive field H_C and saturation magnetization M_{sat}. However, for materials with sufficiently high H_C values ($H_C > 2\pi M_{sat}$) the theoretical limit for the energy product is limited only by M_{sat} and is given by $(BH)_{max} \leqslant (2\pi M_{sat})^2$. The maximum corresponds to an ideal rectangular hysteresis loop. Driven by this limitation, research has focused on developing new high-anisotropy materials with high M_{sat} and Curie temperature T_C. These materials are usually a binary or ternary rare earth (RE)–transition metal (TM) intermetallic, boride or nitride compounds such as $SmCo_5$, Sm_2Co_{17}, $Nd_2Fe_{14}B$, and $Sm_2Fe_{17}N_3$ [1–3]. In these materials, the anisotropy arises predominantly from the crystal-field interaction of the aspherical RE 4f shells while the TM (usually Fe or Co) contribute to higher M_S and T_C. Thus, new hard-magnet compounds are increasing TM rich to enhance M_{sat}. Unfortunately, these

* Corresponding author. Tel.: +1-408-927-2430; fax: +1-408-927-2100.
E-mail address: eef@almaden.ibm.com (E.E. Fullerton)

0304-8853/99/$ - see front matter
PII: S0304-8853(99)00376-5

compounds still have magnetization values significantly lower[1] than that of Co, Fe or $Fe_{65}Co_{35}$, which have $4\pi M_{sat}$ values of 18, 21, and 24 kG, respectively.

Given these limitations, Kneller and Hawig [4] proposed an alternative approach to enhance the TM content (and therefore increase M_{sat}) by making a nanocomposite of exchange-coupled hard and soft magnetic phases. Such magnets are referred to as 'exchange-spring' or 'exchange-hardened' magnets and provide a pathway to increased $(BH)_{max}$. The hard phase provides the requisite magnetic anisotropy and stabilizes the exchange-coupled soft phase against demagnetization. This type of material was first observed by Coehoorn et al. [5] in a melt-spun $Nd_{4.5}Fe_{77}B_{18.5}$ sample that, when annealed, consisted of a mixture of $Nd_2Fe_{14}B$, Fe_3B and Fe phases. These samples exhibited desirable hard-magnet properties even though they consisted of 85% soft phases (Fe_3B and Fe) and only 15% hard phase ($Nd_2Fe_{14}B$). The lower RE content of these materials have the additional advantage of reducing the costs and improving the corrosion resistance. Skomski and Coey explored the theory of exchange coupled films and predicted that a giant energy product of 120 MGOe (about three times that of commercially available permanent magnets) might be attainable by exploiting the exchange-spring mechanism in *oriented* nanostructured magnets [3,6].

Future applications of exchange-spring magnets will likely be based on a nanodispersed composite geometry obtained in bulk processing [7]. Such exchange-spring magnets have been fabricated mainly by rapid-quenching and subsequent annealing or mechanical alloying to form a nanocomposite with randomly oriented hard grains (see for example Refs. [4,5,8–13]). These materials tend to be isotropic. The measured maximum energy products are improved over isotropic single-phase RE-TM magnets but are still significantly lower than that predicted by theory and less than that of oriented single-phase RE-TM magnets. The microstructural complexities in the random composites often makes understanding their demagnetization behavior and optimizing the hard-magnet properties difficult.

[1] The $4\pi M_s$ values for $SmCo_5$, Sm_2Co_{17}, $NdFe_{14}B$, and $Sm_2Fe_{17}N_3$ are 11.4, 12.5, 16.0 and 15.4 kG, respectively.

To better understand the magnetic properties of exchange-spring magnets, hard/soft magnetic heterostructures such as coupled bilayers and multilayers provide convenient model systems. Thin-film growth allows control of the layer thickness values as well as provides a means for crystallographic alignment of the hard phase as suggested by Skomski and Coey [6]. In addition, because the layered structure results in variations in the magnetic properties predominantly along the growth direction, they can often be more easily modeled as one-dimensional structures. Combined with numerical modeling, these systems allow us to obtain greater insights into the coercivity mechanism and magnetization reversal process in exchange-spring magnets, and to realistically estimate the ultimate gain in performance that can potentially be realized in permanent magnets based on the exchange hardening principle.

In this paper, we review the research on modeling, fabrication and characterization of exchange-spring coupled magnetic films and multilayers. We will highlight our recent work on epitaxial SmCo/Fe and SmCo/Co bilayers and superlattices that display many of the characteristic features of exchange-spring magnets. The epitaxy allows for the preparation of hard magnetic layers with well-defined magnetic anisotropy, both in magnitude and direction. The model exchange-spring magnets are realized by systematically interleaving hard and soft phases into layered structures. The magnetization reversal process is examined experimentally using magnetometry, magneto-optical Kerr effect and Brillouin light scattering, and is compared with numerical solutions of a one-dimensional atomic model. The results indicate that exchange-spring behavior in this system can be primarily understood from the intrinsic parameters of the hard and soft layers. We also extend the numerical simulation to bilayer structures with different combinations of layer thicknesses, and demonstrate the systematics with which the maximum energy product of exchange-spring magnets depends on their configuration. In the final section we briefly discuss the magnetic properties of exchange-spring coupled films that are of interest outside the arena of permanent magnets.

2. Magnetic reversal of exchange-spring magnets

An important issue for assessing the applicability of exchange-spring magnets is the nature of the magnetic reversal processes. That is, how do the dimensions, relative volume fractions, and geometry of the soft and hard phases affect properties such as remanent magnetization, H_C and $(BH)_{max}$ of the composite system? A number of theoretical approaches have been applied to address this problem including deriving analytical expressions [6,14], applying micromagnetic modeling [15–20], as well as first-principles calculations [21,22]. In general, these approaches find that the most important parameters in characterizing the switching behavior is the dimension of the soft phase. For a thin soft-phase layer sandwiched between two hard layers (or a soft-phase inclusion in a hard-phase matrix) there is a critical thickness below which the soft phase is rigidly coupled to the hard phase, and the two phases reverse at the same nucleation field resulting in a rectangular hysteresis loop. For thicker soft layers, the soft phase nucleates the reversal at significantly lower fields and the switching is characterized by inhomogeneous reversal. Although the value of H_N depends on the material parameters of both the hard and soft layers, the critical soft-layer thickness is found to be roughly twice the width of a domain wall δ_h in the hard phase [4,6,18],

$$\delta_h = \pi\sqrt{A_h/K_h},$$

where A_h and K_h are the exchange and anisotropy constants of the hard phase, respectively. Thus, this length scale determines many of the physical properties of these systems independent of sample geometry.

2.1. Soft-layer thickness values $\leqslant \delta_h$

For layer thickness values less than the critical thickness, the two phases are rigidly coupled and the composite system is characterized by the averaged magnetic properties of the two layers and is expected to switch at a nucleation field given by

$$H_N = \frac{2(t_h K_h + t_s K_s)}{t_h M_h + t_s M_s},$$

with anisotropy (K_s and K_h), magnetization (M_s and M_h), and layer thickness values (t_s and t_h) of the soft and hard layers, respectively. If one then assumes a rectangular hysteresis loop with $H_C = H_N$, the maximum energy product is given by $(2\pi M_{ave})^2$ for $H_C > 2\pi M_{ave}$, and $4\pi^2 H_C M_{ave}$ for $H_C < 2\pi M_{ave}$, where $M_{ave} = (t_h M_h + t_s M_s)/(t_h + t_s)$. Under these assumptions ($K_s = 0$), the $(BH)_{max}$ occurs at $H_C = 2\pi M_{ave}$ and is given by

$$(BH)_{max} \approx (2\pi M_s)^2\left[1 - \frac{2\pi(M_s - M_h)M_s}{K_h}\right].$$

Therefore, for large K_h the energy product approaches the value of the theoretical limit of the soft phase with a hard phase volume fraction of only $\sim \pi M_s^2/K_h$ [6].

Skomski and Coey make a better estimate of $(BH)_{max}$ for multilayer structures and derived an implicit equation that can be solved numerically to determine the nucleation field H_N of a hard/soft multilayer in terms of the exchange constants (A_s and A_h), anisotropy constants, magnetization, and layer thicknesses of the soft and hard layers:

$$\sqrt{X}\tanh[t_h\sqrt{X}/2] = \frac{A_s}{A_h}\sqrt{Y}\tan[t_s\sqrt{Y}/2],$$

where $X = (2K_h - 4\pi M_h H_N)/2A_h$ and $Y = 4\pi M_s H_N/2A_s$. From these expressions they conclude that a $Sm_2Fe_{17}N_3/Fe_{65}Co_{35}$ multilayer with $t_h = 2.4$ nm and $t_s = 9.0$ nm has a potential $(BH)_{max}$ of 120 MGOe with only a 5 at% Sm content. Similar calculation have predicted $(BH)_{max}$ values of 90 MGOe for $Nd_2Fe_{14}B/Fe$ [18] and FePt/Fe [22] multilayers, 74 MGOe for Sm_2Co_7/Fe [23] and 65 MGOe for $SmCo_5/Fe_{65}Co_{35}$ [21]. In all these cases the energy product is significantly increased over the value of the hard phase which highlights the potential of the exchange-hardening principle.

2.2. Soft-layer thickness values $> \delta_h$

For thicker soft layers, the coercivity of the soft layers drops quickly, which degrades the hard-magnet properties of composite systems. This arises because the soft layer nucleates reversal at fields well below that of the hard layer. The switching of

a soft-magnet film coupled ferromagnetically to a hard layer was first studied in the middle 1960s by Goto et al. [24] and Thompson [25]. Under the assumption that the hard layer is perfectly rigid and $K_s = 0$, they solved for the magnetization of the soft layer with an applied field opposed to the hard layer. They determined that the soft layer remains parallel to the hard layer for fields less than the nucleation field (or the exchange field H_{ex}) given by

$$H_{ex} = \pi^2 A_s / 2 M_s t_s^2.$$

Micromagnetic calculations that include a finite anisotropy of the hard layer find that H_{ex} scales as $t_s^{-1.75}$ for thicker soft layers [18]. This can be compared to $d_s^{-0.701}$ scaling for a spherical soft inclusions in a hard phase where d_s is the diameter of the inclusion [19].

Once the magnetic field exceeds H_{ex} magnetic reversal proceeds via a twisting of the magnetization in the soft layer. This occurs because the soft layers are strongly pinned at the interface while the center of the soft layer is free to follow the external field. This is shown schematically in Fig. 1 for a hard/soft magnetic bilayer. For $H > H_{ex}$, the spins in the soft layer exhibit continuous rotation, as in a Bloch wall, with the angle of rotation increasing with increasing distance from the hard layers. Such magnets exhibit reversible demagnetization curves since the soft layers rotate back into alignment with the hard phase if the reverse field is removed. This reversing process is often referred to as an exchange-spring process by analogy with the elastic motion of a mechanical spring.

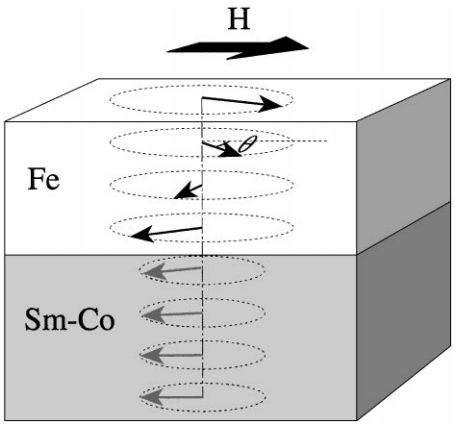

Fig. 1. Illustration of an exchange-spring state in a hard-magnetic/soft-magnetic bilayer.

3. Exchange-spring films and superlattices

The experimental research on hard/soft magnetic films and multilayers have focused mainly on either of two fundamental topics: (i) the potential of enhancing $(BH)_{max}$ via the exchange hardening mechanism or (ii) to explore the physics of the exchange-spring reversal processes. As discussed above, significantly enhancing $(BH)_{max}$ requires both the hard and soft layer thickness values stay $\leqslant \delta_h$. This requires the growth of nanometer-scale permanent-magnet films [26,27] and their incorporation into suitable magnetic heterostructures. Example of structures that have been synthesized include Sm–Co/FeCo films [28], Pr–Co/Co films [29,30], α-Fe/Nd–Fe–B films and multilayers [31–33], Sm–Co/Co multilayers [34,35] and FePt/Fe multilayers [36,37]. Although many of these structures exhibit exchange-hardening phenomena they often differ from the model structures discussed above. For example, the FePt/Fe structures achieve very high $(BH)_{max}$ values >40 MGOe [37]. However, because the samples are produced by rapid thermal annealing of Fe/Pt multilayers, the resulting film is a nanostructured material that no longer exhibits the original multilayer structure. Similarly, the lack of easy-axis alignment of the hard phase in many of the structures makes detailed comparisons with theory difficult. The growth of epitaxial, elemental transition metal films and superlattices has proven essential in elucidating the role of crystal orientation and microstructure on magnetic properties such as giant magnetoresistance and interlayer coupling [38]. Extending this approach allows for the preparation of RE-TM permanent magnet layers with well-defined magnetic anisotropy [39], that can be used as the building blocks for model exchange-spring magnets. As an example, we will discuss the growth and magnetic properties of epitaxial Sm–Co films and heterostructures.

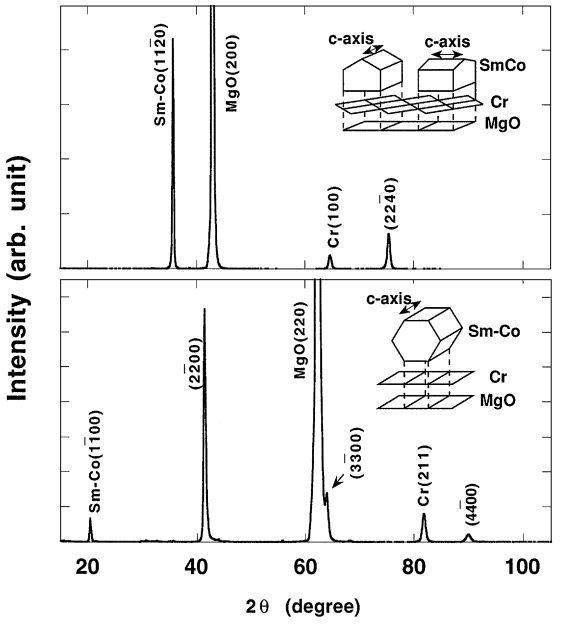

Fig. 2. X-ray diffraction patterns of Sm–Co grown epitaxially via sputtering on Cr-coated single-crystal MgO substrates. The insets illustrate the epitaxial relations: the (1 1 $\bar{2}$ 0)-oriented Sm–Co has a twinned bi-crystal structure and (1 $\bar{1}$ 0 0)-oriented Sm–Co is uniaxial. The Sm–Co *c*-axis, which is the magnetic easy axis, lies in-plane.

3.1. Epitaxial Sm_2Co_7 hard-magnet films

We have grown epitaxial Sm–Co films by magnetron sputtering onto Cr-coated MgO substrates [26]. The 200 Å Cr buffer layers are deposited onto single-crystal MgO(1 0 0) and (1 1 0) substrates at a substrate temperature T_S of 600°C resulting in Cr(1 0 0) and (2 1 1) epitaxial growth, respectively. The Sm–Co films are subsequently deposited with a nominally Sm_2Co_7 composition by co-sputtering from separate elemental Sm and Co sources.

Shown in Fig. 2 are the X-ray diffraction patterns of 1500 Å thick Sm–Co films deposited simultaneously onto Cr(1 0 0) and (2 1 1) buffer layers. For each buffer layer, a single orientation of the Sm–Co film is stabilized. The diffraction patterns are consistent with *a*-axis (1 1 $\bar{2}$ 0) and *b*-axis (1 $\bar{1}$ 0 0) Sm–Co growth onto Cr(1 0 0) and (2 1 1), respectively. These orientations are the same as those observed for Co films on Cr(1 0 0) and (2 1 1) buffers [40]. The insets illustrate the epitaxial relations. In both cases, the Sm–Co *c*-axis, which is the magnetic easy axis, lies in-plane. The *a*-axis Sm–Co films on Cr(1 0 0) buffer layers grow with a twinned epitaxy, as there are two ways to place the HCP Sm–Co unit cell onto the Cr(1 0 0) surface template. The two epitaxial relations are Sm–Co[0 0 0 1]||Cr[0 1 1]||MgO[0 1 0] and Sm–Co[0 0 0 1]||Cr[0 1 $\bar{1}$]||MgO[0 0 1]. The epitaxial relation for the *b*-axis Sm–Co films on Cr(2 1 1) is Sm–Co[0 0 0 1]||Cr[0 1 $\bar{1}$]||MgO[0 0 1].

The different crystal orientations lead to distinct magnetic behaviors. The twinning in *a*-axis Sm–Co films causes the *c*-axis of different crystallites to lie in two orthogonal in-plane directions [41]. The twinned crystallites are strongly exchange coupled, giving rise to an effective fourfold in-plane anisotropy. On the other hand, the *b*-axis Sm–Co is uniaxial, showing a square easy-axis loop and a sheared hard-axis loop. The anisotropy fields, estimated from extrapolating the hard-axis loop to saturation, are $\sim$ 20–25 T. These values are comparable to those reported for bulk $SmCo_5$ (25–44 T) [42]. For both orientations large room-temperature H_C values (>3 T) are observed. High-resolution electron microscopy studies show that films of both orientations consist of a mixture of $SmCo_3$, Sm_2Co_7, and $SmCo_5$ polytypoids [41]. The resulting stacking disorder and concomitant variation in local anisotropy constants may give rise to the large H_C values. The difference in the thickness dependence of H_C values for the two crystallographic orientations may arise from additional contributions from the high density of twin boundaries observed in *a*-axis Sm–Co films. The formation of twin boundaries is controlled by the Sm–Co nucleation and is rather insensitive to film thickness. For the *b*-axis Sm–Co films, the coercivity varies logarithmically with thickness, increasing to 4.1 T for the 75 Å films [26]. The anisotropy fields are not strongly thickness dependent, which points toward changes in the microstructure with increasing thickness being responsible for the changes in H_C. The H_C values increase on cooling and vaules as high as 7 T have been measured at 4.2 K.

3.2. Sm–Co/Co superlattices

Shown in Fig. 3 is the dark-field cross-sectional TEM images of a [Sm–Co(450 Å)/Co(300 Å)]$_{10}$ superlattice deposited onto a MgO(1 0 0) substrate with a Cr(1 0 0) buffer layer [34]. The image shows the layered structure with well-defined boundaries between the Sm–Co and Co layers. Also shown in Fig. 3 is the electron-diffraction pattern from the same film. Because of the twinning, the electron beam is parallel to both [0 0 0 1] and [1 0 $\bar{1}$ 0] zone axes of the HCP structure; the diffraction pattern consists of two sets of projections with both six-fold and two-fold symmetry. The twinning observed in single *a*-axis Sm–Co films is also evident in the dark-field micrograph of the superlattice as the boundaries within the layers. In some regions the twinning extends through several layers, indicative of the structural coherence of the superlattice. Since the Sm–Co/Sm superlattices are structurally coherent, all the Sm–Co and Co layers must have the same easy-axis direction. In this sense, the ideal structure of an aligned exchange-spring magnet is realized in the superlattice films.

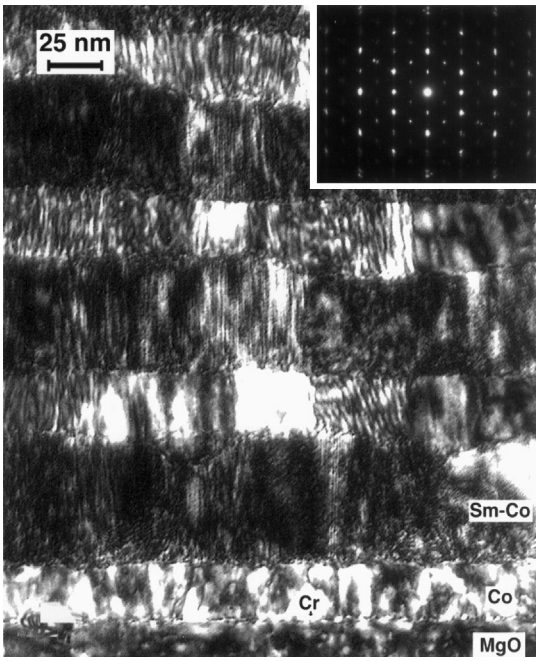

Fig. 3. Dark-field cross-sectional TEM micrographs and the electron diffraction pattern of a (1 1 $\bar{2}$ 0)-oriented Sm–Co/Co superlattice.

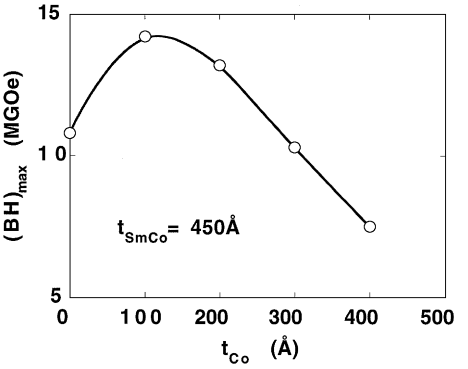

Fig. 4. Maximum energy-product $(BH)_{max}$ of a series of Sm–Co/Co superlattices as a function of Co layer thickness. The curve is a guide to the eye.

Shown in Fig. 4 is the room-temperature maximum energy product $(BH)_{max}$ extracted from the measured hysteresis loops for a series of Sm–Co/Co superlattices with fixed Sm–Co layer thickness plotted as a function of the Co layer thickness. Although a single Sm–Co layer has coercivity as large as 3 Tesla, the low saturation magnetization of Sm_2Co_7 leads to a $(BH)_{max}$ of just 11 MGOe. When interleaved with Co layers, the total saturation magnetization of the multilayer initially increases, and $(BH)_{max}$ increases by as much as 30% to $\sim$ 14 MGOe. Although the value of $(BH)_{max}$ is relatively low, the large percentage change in $(BH)_{max}$ clearly reflects the benefit of the exchange-spring principle. Upon further increase of the Co layer thickness, the coercivity of the superlattices decreases. Even though the total saturation magnetization still increases, the softening of the magnetic properties degrades the $(BH)_{max}$. Thus, to realize the full potential of the exchange-spring magnets, one needs to understand the magnetization reversal process and identify factors that affect the demagnetization.

3.3. Sm–Co/Fe bilayer structures

The simplest structure that embodies the exchange-spring principle is a bilayer for which the soft and hard magnet layers are exchange-coupled

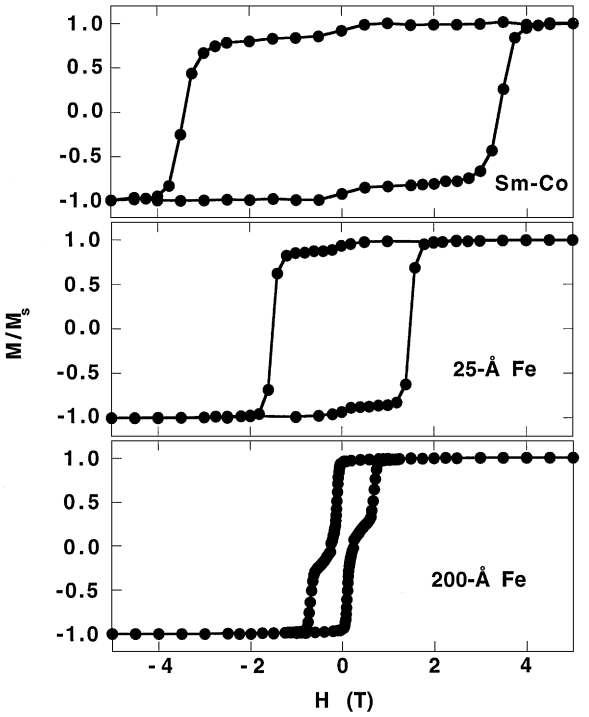

Fig. 5. Room-temperature hysteresis loops of a single Sm–Co film and Sm–Co/Fe bilayers with different Fe layer thicknesses.

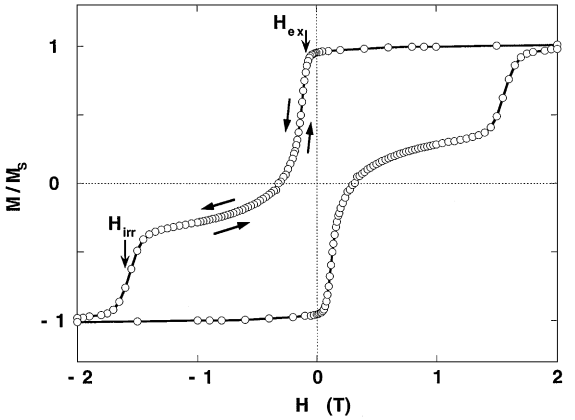

Fig. 6. Low-temperature (25 K) hysteresis loop for the SmCo/Fe(200 Å) sample shown in Fig. 5. The recoil curve shows the 'exchange-spring' behavior of the sample. The Fe magnetization is pinned at the interface by the underlying Sm–Co layer and is fully reversible before the Sm–Co layer switches at H_{irr}.

at the interface. We have prepared Sm–Co/Fe bilayers on single-crystal MgO(1 1 0) substrates coated with an epitaxial 200 Å Cr(2 1 1) buffer layer [23,43]. Because of epitaxy, the Sm–Co layer is (1 $\bar{1}$ 0 0)-oriented, with a $\sim$25 Tesla uniaxial in-plane anisotropy. The magnetically soft Fe layer is polycrystalline with a (1 1 0) texture.

Shown in Fig. 5 are the magnetic hysteresis loops for a single *b*-axis Sm–Co film and Sm–Co/Fe bilayers with 25 and 200 Å Fe. The hysteresis loops are measured with the field H applied along the easy axis direction (MgO[0 0 1]). For the Sm–Co single layer, a square loop is observed with a coercive field H_C of 3.4 T. The Sm–Co saturation magnetization is $\sim$500–600 emu/cm^3. For the bilayer with a 25 Å Fe layer, the loop shape is similar to that of a single Sm–Co layer. A square easy-axis loop is measured, indicating that the entire Fe layer is strongly coupled to the underlying Sm–Co film and that the two layers switch as a unit. Compared to the single Sm–Co film, the coercivity of the bilayer is reduced by $\sim$50% to 1.7 T. This result agrees with the observation of SmCo/FeCo bilayers of Ref. [28]. For the bilayer with a 200 Å Fe layer, the loop changes shape quite significantly. The Fe layer nucleates reversal at a field ($H_N = 0.09$ T) well below the field required to reverse the Sm–Co layers. The subsequent switching field for the Sm–Co layer (0.6–0.7 T) is only 20% of that of a single Sm–Co film.

One characteristic of exchange-spring magnets is that since the soft and hard phases are only exchange-coupled at the interface, the reorientation of the soft layer should be fully reversible for fields below the switching field of the hard layer (see Fig. 1). This behavior is demonstrated for the SmCo/Fe(200 Å) sample. Shown in Fig. 6 is the easy-axis hysteresis loop as well as a minor loop up to 1.2 T. The Fe layer starts to switch at $H_N = 0.09$ T. Above H_N, a sharp drop in the magnetization is then followed by an asymptotic approach to saturation until the hard layer switches irreversibly at H_{irr}. The minor loop shows that the switching of the Fe layer is completely reversible for fields as large as 1.2 T. This characteristic shape and reversible exchange-spring behavior has been observed in a variety of hard/soft bilayer systems.

These include the original study of electroplated NiCo/NiFe bilayers by Goto et al. [14] and later studies on amorphous SmCo/NiFe [44,45] and SmCo/CoZr [46,47], and epitaxial $CoFe_2O_4$/$(Mn,Zn)Fe_2O_4$ exchange-coupled films [48]. For the SmCo/NiFe and SmCo/CoZr films, uniaxial anisotropy was achieved by deposition or annealing of the amorphous SmCo layer in an external field. In all these studies, $t_s > 500$ Å and the hard layer switching fields were lower than the SmCo/Fe example.

3.4. Numerical simulation

For bilayer samples with uniaxial anistropy, it is often possible to obtain considerable insight into the switching of both the soft and hard layers by comparing the magnetization data with one-dimensional atomic models [14,23,44,47]. The composite film is treated as a chain of spins normal to the layers and each spin is the sum of total moments in an atomic layer (see Fig. 1). The total energy of the system is given by

$$E = -\sum_{i=1}^{N-1} \frac{A_{i,i+1}}{d^2}\cos(\theta_i - \theta_{i+1}) - \sum_{i=1}^{N} K_i \cos^2(\theta_i) - \sum_{i=1}^{N} HM_i \cos(\theta_i - \theta_H), \quad (1)$$

where the rotation angle for the ith atomic layer θ_i is measured relative to the easy-axis direction of the hard layer, θ_H is the angle between the field and the easy axis, A_i, K_i, M_i, d are the exchange constants, uniaxial anisotropy constants, magnetic moments and inter-plane distance (set to 2 Å for our examples), respectively. The equilibrium spin configuration for a given field is determined by minimizing Eq. (1) by an iterative approach outlined by Camley [49]. Details of the modeling are in Ref. [23]. In general, the parameters for K and M can be determined from measurements of single hard and soft films. This leaves the exchange parameters as the only unknown constants.

Shown in Fig. 7a is the comparison of the calculated Sm–Co/Fe(200 Å) demagnetization curves to the one shown in Fig. 6. Included are both the longitudinal and transverse magnetization with respect to the applied field. The parameters used in the calculation are, for the hard layer, $A_h = 1.2\times10^{-6}$ erg/cm, $K_h = 5\times10^7$ erg/cm^3, $M_h = 550$ emu/cm^3; for the soft layer, $A_s = 2.8\times10^{-6}$ erg/cm, $K_s = 10^3$ erg/cm^3, $M_s = 1700$ emu/cm^3, the interface exchange constant $A_{int} = 1.8\times10^{-6}$ erg/cm and $\theta_H = 3°$. The values of K_h and M_h were estimated from magnetization measurements on the Sm–Co films. The calculation reproduces the H_{ex} value, the field dependence of both the longitudinal and transverse magnetization, as well as the switching field of the Sm–Co layer at ~ 1.5 T.

The demagnetization curve is most sensitive to A_s and, therefore, these structures provide an experimental determination of the exchange parameter of the soft overlayers. The experimental value

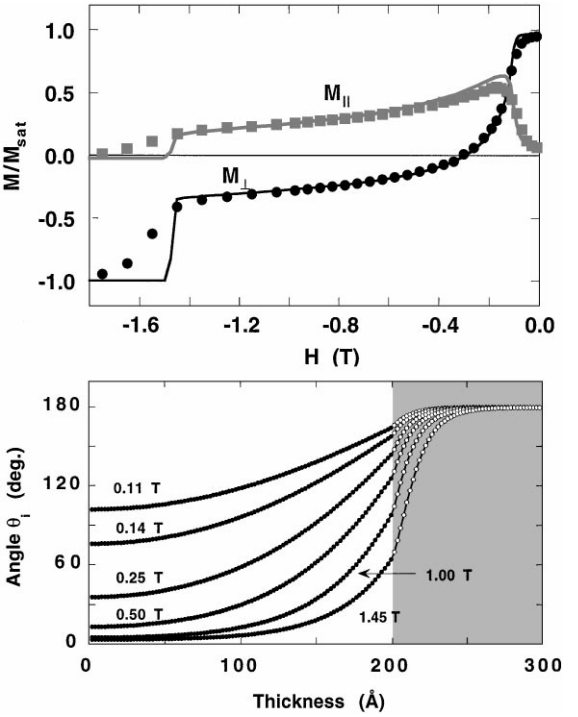

Fig. 7. (a) (top) Demagnetization curves (longitudinal component $M_{||}$, and transverse component $M_\perp$) of a Sm–Co/Fe(200 Å) bilayer structure. The solid curves are results of numerical calculations using the intrinsic parameters of the individual layers. Schematic illustration of the one-dimensional atomic model used in the numerical simulation is shown in Fig. 1. (b) (bottom) Calculated equilibrium spin configuration of a Sm–Co/Fe(200 Å) bilayer structure at several reversal fields.

determined (2.8×10^{-6} erg/cm) compares favorably with the tabulated value for α-Fe of 2.5×10^{-6} erg/cm [50] and the value 2.6×10^{-6} emu/cm determined for NiFe overlayers [45]. Because the exchange-field scales as $A_s/M_s t_s^2$, the major uncertainties in determining A_s results from uncertainties in t_s and M_s. The value of A_{int}, which is intermediate to the exchange coupling of the hard and soft layers, reflects the strong interfacial exchange coupling between the layers expected for ferromagnetic exchange. With a large interfacial exchange energy, the moments in the soft layer near the interface are pinned by the hard layer. Shown in Fig. 7b is the spin configuration at several reversal fields for the calculated magnetization in Fig. 7a. As expected, the distribution of moments is consistent with the expectation that the Fe located away from the interface rotates more as in a Bloch wall.

As H increases, the Bloch wall in the Fe layer is compressed against the Sm–Co layer and the interfacial Sm–Co spins are also increasingly rotated. At a field such that the domain wall energy density in the soft layer becomes greater than that in the hard layer, the domain wall in the soft layer moves into, and switches, the hard layer via domain wall motion. However, this type of domain-wall motion is very different from that observed in an isolated SmCo film. In such films the domain walls separate regions with opposite magnetization directions, propagate horizontally across the film and are pinned by local variation in the magnetic properties. In the exchange-spring structures, the domain wall propagates from the top of the hard layer to the bottom. The nature of the domain wall pinning is expected to be significantly reduced in the vertical directions which may explain the close agreement for the SmCo switching field even though no microstructural features are included in the calculations. The same parameters also reproduce the evolution of the magnetic properties, both reversible and irreversible with decreasing Fe thickness [23].

With these parameters we can simulate a series of hysteresis loops for bilayers with different Fe and Sm–Co layer thickness values and extract the maximum energy product $(BH)_{max}$. Shown in Fig. 8 are the calculated $(BH)_{max}$ curves plotted as a function of Fe layer thickness for different Sm–Co layer thicknesses. $(BH)_{max}$ increases initially with increasing Fe thickness, peaks, and then decreases. The peak value of $(BH)_{max}$ increases with decreasing Sm–Co thickness. Also shown as dashed curves is the ideal energy product $(BH)_{max} = (2\pi M_{sat})^2$. At low Fe thicknesses (less than the Bloch wall width in the hard layer), the Fe layer couples rigidly to the hard layer and the nucleation field is greater than $2\pi M_{sat}(BH)_{max}$ then increases as a result of the increased saturation magnetization, following the ideal curve. With increasing thickness, the Fe-layer magnetization reverses at lower fields, and $(BH)_{max}$ is limited by H_N. The square symbols are the $(BH)_{max}$ values taken from the measured hysteresis loops of the Sm–Co/Fe bilayer films. The model calculation agrees with the experimental data reasonably well, it also resembles the $(BH)_{max}$ curve of the Sm–Co/Co superlattices. The calculation shows that for bilayers with suitably thin constituent layers, $(BH)_{max}$ can even be greater than that of Nd–Fe–B.

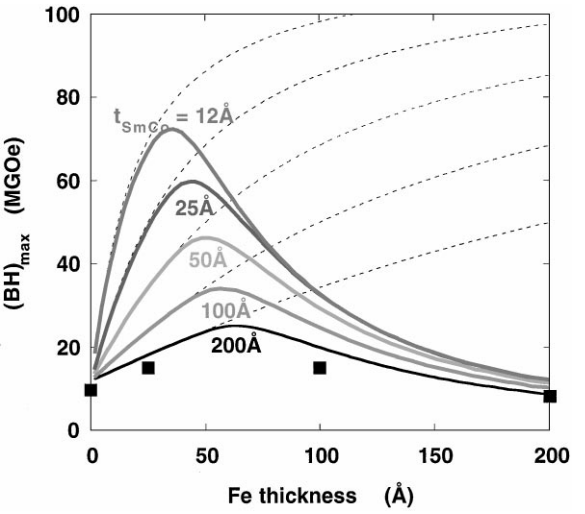

Fig. 8. Calculated maximum energy product $(BH)_{max}$ of Sm–Co/Fe bilayers with different layer thicknesses. The dashed curves are that of the ideal $(BH)_{max} = (2\pi M_s)^2$. The highest $(BH)_{max}$ observed experimentally for Nd–Fe–B magnets is ~ 55 MGOe.

3.5. SmCo/Co layers

Shown in Fig. 9 is the low-temperature demagnetization curve and minor loop for a

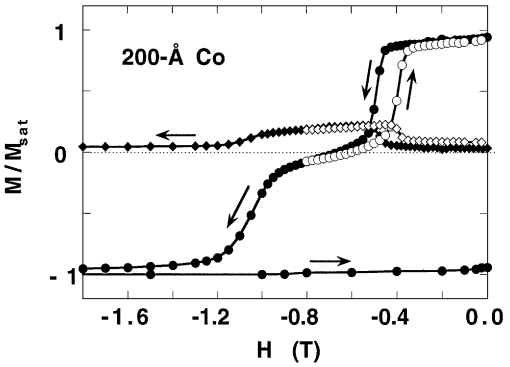

Fig. 9. Low-temperature (25 K) demagnetization curve (solid symbols) for a SmCo/Co(200 Å) sample. We show both the longitudinal (circles) and transverse (diamonds) magnetization components. The open symbols illustrate the recoil curve showing the hysteretic reversal of the Co layer.

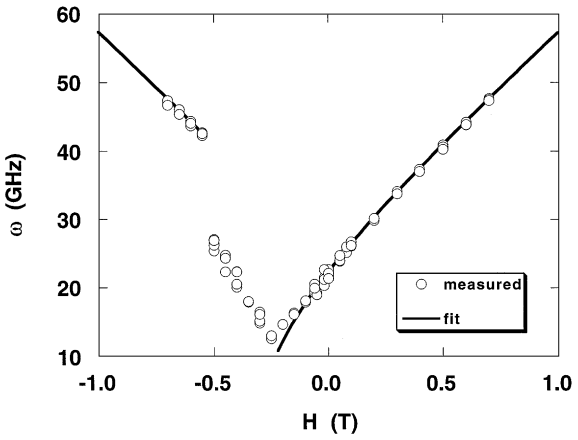

Fig. 10. Magnon frequencies measured using Brillouin light scattering. The solid lines are a fit assuming an effective exchange field in the Fe layer.

SmCo/Co(200 Å) bilayer film. For this film, the switching of the Co layer is reversible but is hysteretic about the exchange field $H_{ex} = 0.46$ T. This value is much higher than the H_{ex} for the SmCo/Fe film. Both the high H_{ex} and hysteretic behavior results from the finite anisotropy of the Co layer. The *c*-axis anisotropy stabilizes the Co layer either parallel or antiparallel to the SmCo layer and results in an abrupt and hysteretic reversal at H_{ex}. Goto et al. discussed this type of film under the approximation that each layer could be treated as uniformly magnetized and coupled by a mechanical spring [24]. Such a model is similar to the proximity magnetism model proposed by Slonczewski [51]. The strength of the coupling should be roughly the energy of a domain wall γ ($\sim 10\,\mathrm{erg/cm^2}$) and an estimate for H_{ex} is given by $\gamma/M_s t = 0.36$ T, in reasonable agreement with the experimental results. Both the hysteretic reversal of the soft layer and the exchange field scaling with t_s^{-1} for a soft layer with finite anisotropy were observed in $(Mn,Zn)Fe_2O_4/CoFe_2O_4$ bilayers [48].

3.6. Magnetic excitations

In addition to the static magnetization of exchange-spring system, the dynamic properties of the system provide a valuable probe of the magnetic properties [52] as well as suggest potential applications for such structures in high-frequency signal processing [53]. Shown in Fig. 10 is the field dependence of the magnon frequency in the Sm–Co/Fe bilayer film with an 100 Å Fe layer measured using Brillouin light scattering (BLS). Due to the finite penetration of light, the BLS signal is dominated by contributions from magnons in the top Fe layer. The frequencies decrease with decreasing H, reaching a minimum at $H = -0.25$ T, and then increase for even lower fields. At $H \sim -0.55$ T, the frequency changes abruptly and become equal to the corresponding positive field value. In the regions below -0.55 T and above -0.25 T, where the magnetization of the Fe layer lies along the easy axis of the Sm–Co and is also either parallel or antiparallel to the applied field, the magnon frequency can be described by the standard magnon theory [54] for an isolated Fe film if we assume that there is an effective exchange field in the Fe layer due to the underlying Sm–Co layer. A more complete description of the magnon frequencies starting from Eq. (1) provides quantitative agreement of both the easy- and hard-axis data and provides strong evidence that the microscopic origin of the spring magnets are well understood [52].

4. Novel magnetic properties of exchange-spring coupled films

A novel feature of exchange-spring systems is the ability to control and manipulate domain-wall structures in ferromagnetic films. Such structures allow a variety of physical phenomena to be explored and parameters such as the exchange constant to be determined. We will briefly highlight some areas where these structures are being exploited.

4.1. Domain-wall magnetoresistance

There has been recent interest in the role that domain walls have on spin-dependent electron transport. This problem was first explored to explain the magnetoresistance effects of Fe whiskers [55] but has gained renewed interest from recent reports of giant magnetoresistance (GMR) effects from domain walls in Co films [56]. Mibu et al. [57] used a SmCo/NiFe exchange-spring structure to explore magnetotransport in NiFe films in the presence of Bloch-wall type structure introduced by an external reverse field. They concluded that the magnetoresistance in their system is dominated by the anisotropic magnetoresistance and that any GMR effect, if present, is significantly smaller, in agreement with recent measurements on Fe wires [58].

4.2. Domain-wall junctions

Domain-wall junctions are structures similar to exchange-spring magnets but consist of two soft layers with a thin hard intermediate layers [59,60]. The aim of research on such structures is to study the behavior of a domain wall interacting with the potential barrier created by the hard layer. The magnetic reversal process is similar to that described for the SmCo/Fe system above. A domain wall nucleates at the top of the film in a reverse field and is pinned at the hard-magnet layer, as in an exchange-spring system. As the reverse field is increased the domain wall compresses against the hard layer and then propagates from the top soft layer into the bottom soft layers. The hard layer acts as a potential barrier separating two regions of low potential and is analogous to a Josephson junction [61]. Such structures have been exploited to study pinning of domain walls in both thermal activation and quantum regimes [59].

4.3. Exchange biasing

The phenomenon of exchange biasing is a property of many antiferromagnetic (AF)/ferromagnetic (F) bilayer systems (see the article by Takano and Berkowitz in this issue). When the sample is cooled through the Néel temperature of the AF layer, the resulting hysteresis loop of the ferromagnetic layer is shift from $H = 0$ by an exchange field H_{ex} arising from a unidirectional magnetic interaction of the ferromagnetic layer with the underlying antiferromagnet. The simple picture suggests that this phenomenon arise solely from the interfacial interaction at the F–AF interface. However, this simple picture is not able to explain the order of magnitude of H_{ex} and other experimental features. More realistic models have been proposed to explain this phenomenon that involve the development of domain walls in the AF and F layers [62] and recent experiments have shown evidence for twisted magnetic structure [63,64]. In this way, much of the physics and reversal mechanisms are similar to that observed in exchange-spring magnets where the hard layer replaces the AF layer as the biasing layer. The minor loop for the Sm–Co/Co bilayer shown in Fig. 9 resembles the exchange-bias loops of many systems. The main difference is that the minor loop in the exchange spring system has the additional ferromagnetic contribution of the hard layer. The Sm-Co/Co minor loops (as well as the hard-axis loops [23]) are also in qualitative agreement with calculated loops in Ref. [62] that predict an exchange field $H_{ex} = \gamma/M_s t_s$. Such calculations are in reasonable agreement with the exchange field for the Sm–Co/Co bilayers as discussed in Section 3.5. Evidence for exchange-bias phenomena has also been observed in GdFe/TbFe/GdFe domain-wall junctions that is related to the compression and decompression of the domain wall at the GdFe/TbFe interface [60]. Thus, exchange-spring systems may provide model systems that complement our understanding of the exchange-bias problem. In fact, this close agreement has been

exploited in a recent theory that directly models the exchange-bias system as an exchange-spring magnet [65].

5. Conclusions

Model exchange-spring magnets have been realized by systematically interleaving hard and soft magnetic phases into layered structures. Such structures allow the magnetization reversal processes to be examined experimentally and compared quantitatively with theoretical expectations. The results indicate that exchange-spring behavior can be understood from the intrinsic parameters of the hard and soft magnetic phases. Besides revealing the fundamental aspects of the magnetization reversal in exchange-spring magnets, these model systems also address the microstructural influences on the hard magnetic properties. It also realistically estimates the ultimate performance achievable based on the exchange-hardening mechanism, and serves as a guideline for the development of more complex nanostructures with optimized properties.

Acknowledgement

Work at ANL was supported by U.S. DOE BES-MS under Contract No. W-31-109-ENG-38.

References

[1] J.F. Herbst, Rev. Mod. Phys. 63 (1991) 819.
[2] K.H.J. Buschow, Rep. Prog. Phys. 54 (1991) 1123.
[3] J.M.D. Coey, R. Skomski, Phys. Scripta T49 (1993) 315.
[4] E.F. Kneller, R. Hawig, IEEE Trans. Magn. 27 (1991) 3588.
[5] R. Coehoorn, D.B. de Mooij, C. De Waard, J. Magn. Magn. Mater. 80 (1989) 101.
[6] R. Skomski, J.M.D. Coey, Phys. Rev. B 48 (1993) 15812.
[7] J.M.D. Coey, Solid State Commun. 102 (1997) 101.
[8] J. Ding, P.G. McCormick, R. Street, J. Magn. Magn. Mater. 124 (1993) L1.
[9] J. Ding, Y. Liu, R. Street, P.G. McCormick, J. Appl. Phys. 75 (1994) 75.
[10] L. Withanawasam, G.C. Hadjipanayis, R.F. Krause, J. Appl. Phys. 75 (1994) 6646.
[11] L. Withanawasam, Y.H. Zheng, G.C. Hadjipanayis, R.F. Krause, Scripta Metal. et Mater. 33 (1995) 1765.
[12] J. Wecker, K. Schnitzke, H. Cerva, W. Grogger, Appl. Phys. Lett. 67 (1995) 563.
[13] K. ODonnell, J.M.D. Coey, J. Appl. Phys. 81 (1997) 6310.
[14] E. Goto, N. Hayashi, T. Miyashita. K. Nakagawa, J. Appl. Phys. 36 (1965) 2951.
[15] T. Schrefl, J. Fidler, H. Kronmüller, Phys. Rev. B 49 (1994) 6100.
[16] R. Fischer, T. Schrefl, H. Kronmüller, J. Filder, J. Magn. Magn. Mater. 150 (1995) 329.
[17] R. Fischer, H. Kronmüller, Phys. Rev. B 54 (1996) 7284.
[18] T. Lieneweber, H. Kronmüller, J. Magn. Magn. Mater. 176 (1997) 145.
[19] R. Fischer, T. Schrefl, H. Kronmüller, Phys. Rev. B 57 (1998) 10723.
[20] W. Rave, K. Ramstöck, J. Magn. Magn. Mater. 171 (1997) 69.
[21] R.F. Sabiryanov, S.S. Jaswal, Phys. Rev. B 58 (1998) 12071.
[22] R.F. Sabiryanov, S.S. Jaswal, J. Magn. Magn. Mater. 177–181 (1998) 989.
[23] E.E. Fullerton, J.S. Jiang, M. Grimsditch, C.H. Sowers, S.D. Bader, Phys. Rev. B 58 (1998) 12193.
[24] E. Goto, N. Hayashi, T. Miyashita, K. Nakagawa, J. Appl. Phys. 36 (1965) 2951.
[25] D.A. Thompson, Ph. D. Thesis, Carnegie Institute of Technology, Sept. 1965.
[26] E.E. Fullerton, J.S. Jiang, Christine Rehm, C.H. Sowers, Bader S.D., J.B. Patel, X.Z. Wu, Appl. Phys. Lett. 71 (1997) 1579.
[27] D.J. Keavney, E.E. Fullerton, J.E. Pearson, S.D. Bader, IEEE Trans. Magn. 32 (1996) 4440.
[28] I.A. Al-Omari, D.J. Sellmyer, Phys. Rev. B 52 (1995) 3441.
[29] J.P. Liu, Y. Liu, Z.S. Shan, D.J. Sellmyer, IEEE Trans. Magn. 33 (1997) 3709.
[30] J.P. Liu, Y. Liu, D.J. Sellmyer, J. Appl. Phys. 83 (1998) 6608.
[31] M. Shindo, M. Ishizone, H. Kato, T. Miyazaki, A. Sakuma, J. Magn. Magn. Mater. 161 (1996) L1.
[32] M. Shindo, M. Ishizone, A. Sakuma, H. Kato, T. Miyazaki, J. Appl. Phys. 81 (1997) 4444.
[33] S.M. Parhofer, J. Wecker, C. Kuhrt, G. Gieres, L. Schultz, IEEE Trans. Magn. 32 (1996) 4437.
[34] E.E. Fullerton, J.S. Jiang, C.H. Sowers, J.E. Pearson, S.D. Bader, Appl. Phys. Lett. 72 (1998) 380.
[35] J.P. Liu, Y. Liu, R. Skomski, D.J. Sellmyer, J. Appl. Phys. (1999) in press.
[36] J.P. Liu, Y. Liu, C.P. Luo, Z.S. Shan, D.J. Sellmyer, J. Appl. Phys. 81 (1997) 5644.
[37] J.P. Liu, C.P. Luo, Y. Liu, D.J. Sellmyer, Appl. Phys. Lett. 72 (1998) 483.
[38] E.E. Fullerton, M.J. Conover, J.E. Mattson, C.H. Sowers, S.D. Bader, Phys. Rev. B 48 (1993) 15755.
[39] E.E. Fullerton, C.H. Sowers, J.E. Pearson, S.D. Bader, X.Z. Wu, D. Lederman, Appl. Phys. Lett. 69 (1996) 2438.
[40] A. Nakamura, M. Koguchi, M. Futamoto, Jpn. J. Appl. Phys. 34 (1995) 2308.
[41] Mohamed Benaissa, Kannan Krishnan, E.E. Fullerton, J.S. Jiang, IEEE Trans. Magn. 34 (1998) 1204.

[42] K.J. Strnat, R.M.W. Strnat, J. Magn. Magn. Mater. 100 (1991) 38.
[43] J.S. Jiang, E.E. Fullerton, M. Grimsditch, C.H. Sowers, S.D. Bader, J. Appl. Phys. 83 (1998) 6238.
[44] K. Mibu, T. Nagahama, T. Shinjo, J. Magn. Magn. Mater. 163 (1996) 75.
[45] T. Nagahama, K. Mibu, T. Shinjo, J. Phys. D 51 (1998) 43.
[46] D. Givord, J. Betz, K. Mackay, J.C. Toussaint, J. Voiron, S. Wüchner, J. Magn. Magn. Mater. 159 (1996) 71.
[47] S. Wüchner, J.C. Toussaint, J. Voiron, Phys. Rev. B 55 (1997) 11576.
[48] Y. Suzuki, R.B. van Dover, E.M. Gyorgy, J.M. Phillips, R.J. Felder, Phys. Rev. B 53 (1996) 14016.
[49] R.E. Camley, Phys. Rev. B 35 (1987) 3608.
[50] E. Kneller, Ferromagnetismus, Springer, Berlin, 1962.
[51] J.C. Slonczewski, J. Magn. Magn. Mater. 150 (1995) 13.
[52] M. Grimsditch, R. Camley, E.E. Fullerton, J.S. Jiang, S.D. Bader, C.H. Sower, J. Appl. Phys., in press.
[53] R.J. Astalos, R.E. Camley, Phys. Rev. B 58 (1998) 8646.
[54] K.W. Damon, J.R. Eshbach, J. Phys. Chem. Solids 19 (1961) 308.
[55] G.G. Cabrera, L.M. Falicov, Phys. Status Solidi B 61 (1974) 539.
[56] J.F. Gregg, W. Allen, K. Ounadjela, M. Viret, M. Hehn, S.M. Thompson, J.M.D. Coey, Phys. Rev. Lett. 77 (1996) 1580.
[57] K. Mibu, T. Nagahama, T. Shinjo, T. Ono, Phys. Rev. B 58 (1998) 6442.
[58] U. Rüdiger, J. Yu, A.D. Kent, S.S.P. Parkin, Appl. Phys. Lett. 73 (1998) 1298.
[59] S. Mangin, G. Marchal, W. Wernsdorfer, A. Sulpice, K. Hasselbach, D. Mailly, B. Barbara, Europhys. Lett. 39 (1997) 675.
[60] S. Mangin, G. Marchal, C. Bellouard, W. Wernsdorfer, B. Barbara, Phys. Rev. B 58 (1998) 2748.
[61] L. Gunther, B. Barbara, Phys. Rev. B 49 (1994) 3926.
[62] D. Mauri, H.C. Siegmann, P.S. Bagus, E. Kay, J. Appl. Phys. 62 (1987) 3047.
[63] R.D. McMichael, M.D. Stiles, P.J. Chen, W.F. Egelhoff, Phys. Rev. B 58 (1998) 8605.
[64] E.D. Dahlberg, B. Miller, B. Hill, B.J. Jonsson, V. Strom, K.V. Rao, J. Nogues, I.K. Schuller, J. Appl. Phys. 83 (1998) 6893.
[65] M. Kiwi, J. Mejia-López, R.D. Portugal, R. Ramírez, Exchange Bias Model: Role of Domains in the Ferromagnet, preprint.